

# A Study on the Technique of Observing Interplanetary Scintillation with Simultaneous Dual-Frequency Measurements

Xi-Zhen Zhang

National Astronomical Observatories, Chinese Academy of Sciences, Beijing 100012; [zxz@bao.ac.cn](mailto:zxz@bao.ac.cn)

Received 2006 October 8; accepted 2006 December 9

**Abstract** Ground-based observation of Interplanetary Scintillation (IPS) is an important approach of monitoring solar wind speed. We describe both the principle and method of observing the solar wind speed by using the normalized cross-spectrum of simultaneous dual-frequency IPS measurement. The effects of the solar wind properties and the angular size of the scintillation source on the measurement of solar wind speed are investigated by numerical analysis. We carry out a comparison of this method with the traditional single station-single frequency method. We outline a new IPS observation system using this method now under construction at the National Astronomical Observatories, CAS (NAOC).

**Key words:** interplanetary scintillation — method — instrument — telescope

## 1 INTRODUCTION

The main mass in the interplanetary space comes from coronal expansion in the form of inhomogeneous plasma flow (solar wind). The Sun has caused the biggest effects on the Earth in multiple ways. Studying the solar wind impacts not only solar physics, space physics and geophysics, but also the related fields, such as aerospace activities, space communications, safety of humanity, and so on.

Interplanetary scintillation (IPS) is the random fluctuation in the intensity and phase of electromagnetic waves passing through the interplanetary space. The fluctuation is caused by refraction and deflection from the inhomogeneous plasma (solar wind) in the interplanetary space. Observing the IPS using ground based telescopes has given many useful results. Several important IPS stations, such as Cambridge (UK) (Hewish et al. 1964; Purvis et al. 1987), Ooty (India) (Swarup et al. 1971; Manoharan et al. 1990), Puschino (Russia) (Vitkevich et al. 1976), adopted single station- single frequency observations (SSSF) and used the power-spectrum fit method to obtain the solar wind speed and scintillation index, while the STEL (Japan) (Asai et al. 1995) is a multi-station system which can measure the projected solar wind speed directly. The phased array of the Miyun telescope, NAOC, is also an SSSF system operating at 232 MHz (Zhang et al. 2001; Wu et al. 2001). The SSSF mode of IPS observation needs high sensitivity, for example, better than 25 dB, to obtain reasonable spectrum fitting, and the fitting accuracy is somehow easily affected by variations in the solar wind parameters (Ye & Qiu 1996). Another technique of IPS observation using single telescope is the single station dual-frequency method (SSDF) (Scott et al. 1983). This method adopts simultaneous dual-frequency when observing an IPS source and then calculates the normalized cross-spectrum (NCS) with the power spectra of two different frequencies. Comparing to the SSSF mode, the SSDF technique has the following advantages: (1) Higher sensitivity; (2) Higher accuracy on the measurement of solar wind speed; (3) Higher stability against the wide variations in solar wind parameters.

In the present paper, Section 2 shows the principle and method of the SSDF technique. Section 3 introduces our study on the effects from solar wind parameters, the angular size of scintillation source, and the new IPS observational system under construction at the NAOC using the SSDF technique. Finally, a discussion on the effects of solar wind parameters is presented in Section 4.

**Table 1** The minimum distance the weak scintillation condition begins to hold as a function of frequency.

Frequency (MHz)	150	327	900	2000	5000	7500	20000
heliocentric distance $r$ (solar radius)	60	35	18	10	5	4	2

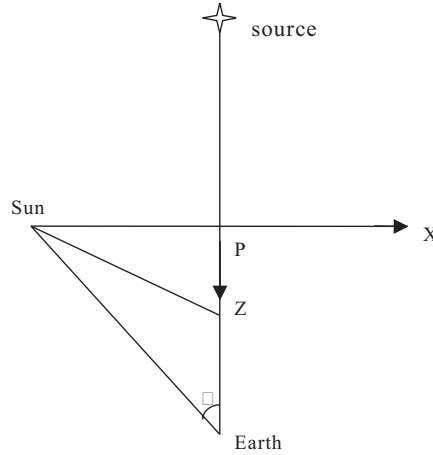


**Fig. 1** IPS geometry.

## 2 THE PRINCIPLE AND METHOD OF THE SSDF IPS OBSERVATION

### 2.1 The Principle

IPS is strong in the space near the Sun, but in most of interplanetary space IPS is weak — the so-called “weak scintillation region”, this is because the IPS amplitude decreases rapidly with increasing heliocentric distance  $r$  as  $r^{-4}$ . The distance where the weak scintillation regime sets in is a function of the frequency. See Table 1. The present study always deals with the weak scintillation condition.

The geometry of IPS is shown in Figure 1. The  $z$ -axis is along the line-of-sight, the  $x$ -axis is in the direction perpendicular to the  $z$ -axis pointing away from the Sun and the  $y$ -axis is normal to the paper.  $P$  is the point closest to the Sun in the line-of-sight,  $r$  is the distance between the Sun and  $P$ ,  $Z$  the distance between  $P$  and the Earth and the angle  $\varepsilon$  is the elongation of Sun-Earth-source.

Equation (1) defines the normalized co-spectrum (NCS) between two simultaneous IPS signals at frequency  $f$ . The NCS is used to acquire the solar wind speed. See Figure 2 for an example of NCS.

$$\text{NCS}(f) = \frac{\text{Re}(S_{12}(f))}{\sqrt{P_1(f) \cdot P_2(f)}}, \quad (1)$$

where  $f$  is the temporal frequency,  $\text{Re}$  denotes the real part of its argument, the co-spectrum  $S_{12}$ , and  $P_1$  and  $P_2$  are the power spectrum at the two frequencies. According to the theory of thin scintillation screen (Ye & Qiu 1996), the correlation between the spatial wave-number and the temporal frequency is  $k_x = 2\pi f/\nu_x$ , then  $S_{12}$ ,  $P_1$  and  $P_2$  can be expressed as follows (Tokumaru et al. 1994):

$$P_i(f) = Cr_e^2 \lambda_i^2 \int_0^\infty \frac{2\pi}{\nu} P(\nu) d\nu \int_{-\infty}^\infty \Phi_{\text{ne}}(\mathbf{k}) \sin^2\left(\frac{k^2 \lambda_i z}{4\pi}\right) \times F_s(\mathbf{k}) F_r(\mathbf{k}) dk_y, \quad (i = 1, 2) \quad (2)$$

$$S_{12}(f) = Cr_e^2 \lambda_1 \lambda_2 \int_0^\infty P(\nu) d\nu \int_{-\infty}^\infty \Phi_{\text{ne}}(\mathbf{k}) \sin\left(\frac{k^2 \lambda_1 z}{4\pi}\right) \sin\left(\frac{k^2 \lambda_2 z}{4\pi}\right) \times F_s(\mathbf{k}) F_r(\mathbf{k}) dk_y, \quad (3)$$

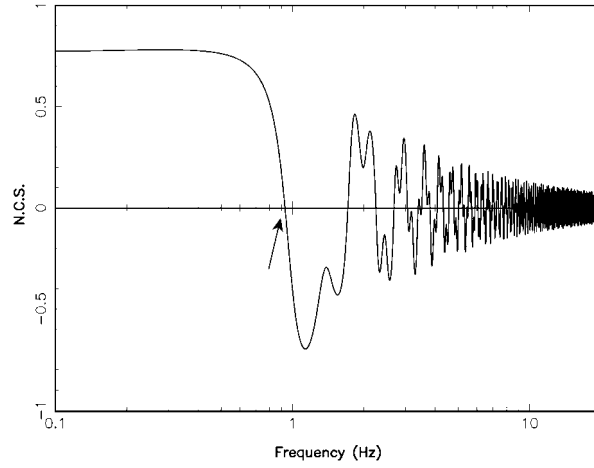


**Fig. 2** An example of NCS. The arrow points to the characteristic frequency,  $f_{zero}$  used in the calculation of the solar wind speed.

where the terms of sin-functions are the Fresnel filters,  $\mathbf{k} = (k_x = 2\pi f/\nu, k_y, k_z = 0)$  is the three dimension wave-number,  $r_e = 2.8 \times 10^{-13}$  cm is the electron radius,  $\lambda_1/\lambda_2$  is the wave-lengths of the two frequencies and  $\lambda_1 > \lambda_2$ ,  $\nu$  the velocity of solar wind along the  $x$  axis at the point  $P$ ,  $P(\nu)$  the distribution function of the solar wind speed, and  $\Phi_{ne}$  the spatial spectrum of the electron density, which is defined in Equation (4),

$$\Phi_{ne}(\mathbf{k}) = Tr^{-4}[(k_x^2 + (k_y/AR)^2)^{-\alpha/2}], \quad (4)$$

where  $T$  is the amplitude of fluctuation of the electron density,  $AR$  the axis ratio which is a measure of the anisotropy of the solar wind,  $r$  the heliocentric distance of the point  $P$ ,  $\alpha$  the index in the solar wind power law and  $F_s$  is the Gaussian cutoff filter to size of the scintillation source (see Equation (5)) (Tokumaru et al. 1994; Ye & Qiu 1996).  $\theta_0$  is the angular diameter of the scintillation source. The brightness distribution of the source is modelled as  $B(\theta) = \exp[-(\theta/\theta_0)^2/2]$ .

$$F_s = \exp[-(k_x^2 + k_y^2)z^2\theta_0^2], \quad (5)$$

$$F_r = \exp\left[-(k_x^2 + k_y^2)/\left(\frac{4\pi \cdot \Delta\lambda}{\lambda^2 \cdot z}\right)^{1/2}\right]. \quad (6)$$

$F_r$  in Equation (6) is the receiver bandwidth ( $\Delta\lambda$ ) filter. The parameters used in the calculation of the exemplar spectrum (Fig. 2) are:  $\nu = 200 \text{ km s}^{-1}$ ,  $\alpha = 11/3$ ,  $AR = 1.0$ ,  $\sigma = 0.0$ ,  $\lambda_1 = 92 \text{ cm}$ ,  $\lambda_2 = 49 \text{ cm}$  and  $Z = 1 \text{ AU}$ . Here  $\sigma$  is the rms fluctuation in the solar wind speed and  $T$  is a constant.

The solar wind speed  $V$  can be obtained from the NCS according to the characteristic frequency  $f_{zero}$  (Tokumaru et al. 1994)

$$V = K f_{zero} \sqrt{\lambda_1 Z}, \quad (7)$$

where  $f_{zero}$  is the first zero of NCS,  $K$  is a correcting factor which varies slightly with the solar wind parameters except when  $\sigma/V$  is large, and it is almost always taken to be 1.1. Table 2 lists the different  $K$  values. For most cases, taking  $K = 1$  will cause no more than 10% error in the measured solar wind speed, which is acceptable.

## 2.2 Effects of Solar Wind Properties and the Angular Size of the Scintillation Source on the NCS

The main parameters of solar wind are  $\alpha$  – power law index of the spatial spectrum of electron density,  $AR$  – axial ratio of solar wind irregularities,  $V$  – solar wind speed, and  $\sigma$  – rms speed fluctuation. To study the effects of these parameters on the NCS several models with different parameters have been calculated.

**Table 2** Factor  $K$  for different solar wind parameters (compiled from the table of Tokumaru et al. 1994).

AR	$\alpha$	$\sigma/V$	$K$
1.0	3.6	0.0	1.12
1.5	3.6	0.0	1.15
2.0	3.6	0.0	1.17
3.0	3.6	0.0	1.19
1.0	2.0	0.0	1.15
1.0	3.0	0.0	1.13
1.0	4.0	0.0	1.11
1.0	3.6	0.1	1.11
1.0	3.6	0.3	1.03
1.0	3.6	0.4	0.96
1.0	3.6	0.5	0.88
1.0	3.6	0.8	0.69

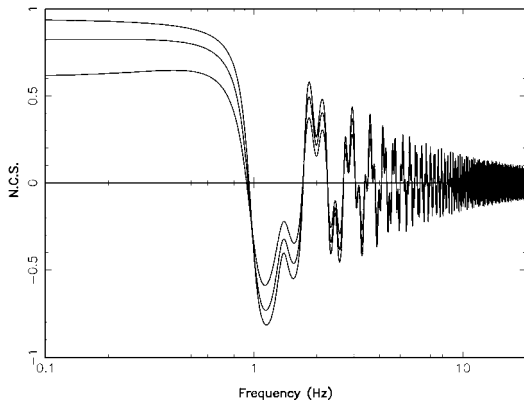


**Fig. 3** NCS for three values of the power law index ( $\alpha$ : 2.5, 3.5, 4.5).

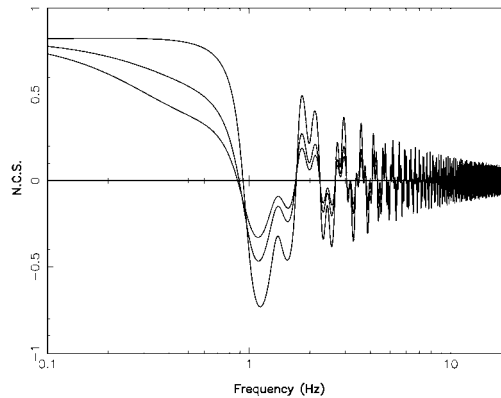


**Fig. 4** NCS for three values of the axial ratio (AR: 1.0, 2.0, 3.0).

Figure 3 shows the NCS for three values of  $\alpha$ , 2.5, 3.5 and 4.5. Although the shape of the NCS varies much for  $f < f_{zero}$  and  $f > f_{zero}$ , a clear result can be found from Figure 3 that the locations of the zeros are almost the same for the three curves. This implies that any errors in the calculated solar wind speed caused by variations of  $\alpha$  are small, even when  $\alpha$  varies by as much as 2.5–4.5. Similarly, Figures 4 and 5 indicate that any variations in either the axial ratio AR (1.0/2.0/3.0) or the angular size of the scintillation source (0.01/0.1/0.2'') have small effects on the calculated solar wind speed by the NCS technique. The NCSs for different solar wind speeds (300/350/400 km s<sup>-1</sup>) are shown in Figure 6. The result derived from Figure 6 is that different solar wind speeds imply obviously different locations of  $f_{zero}$ . The conclusion from Figures 3–6 is that  $f_{zero}$  are sensitive to the solar wind speed. This is in agreement with Equation (7). On the other hand,  $f_{zero}$  are not sensitive to the solar wind parameters  $\alpha$ , AR, or the angular size of the scintillation source. This advantage of the NCS technique is expected.

The study above presumes a uniform solar wind speed distribution. Some author suggested that the solar wind speed distribution also depends on the sampling rate of the receiver and the data length used to obtain the power spectrum, but if the sampling rate is high and the period to calculate spectra is short, then the solar wind speed can be regarded as uniform for a wide range of solar wind parameters.

It is possible that  $f_{zero}$  may increase when the solar wind speed distribution is not uniform ( $\sigma/V \neq 0$ ). To study this possibility some simulations have been done and the results showed that the measurement error of the solar wind is smaller than 10% for a range of solar wind speed distributions ( $0 < \sigma/V < 0.5$ ).

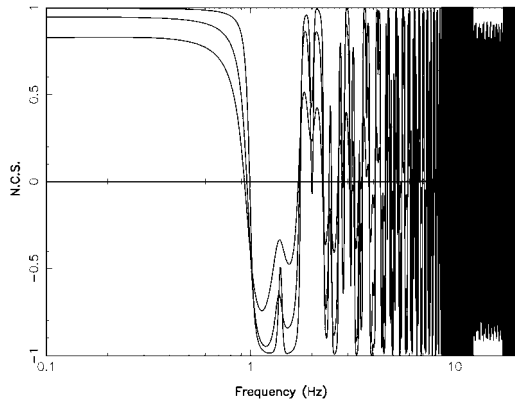


**Fig. 5** NCS for three values of the source angular size (0.01/0.1/0.2'').

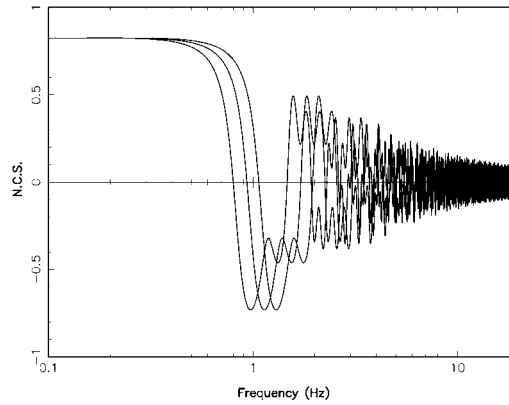


**Fig. 6** NCS for three values of the solar wind speed (300/350/400 km s<sup>-1</sup>).

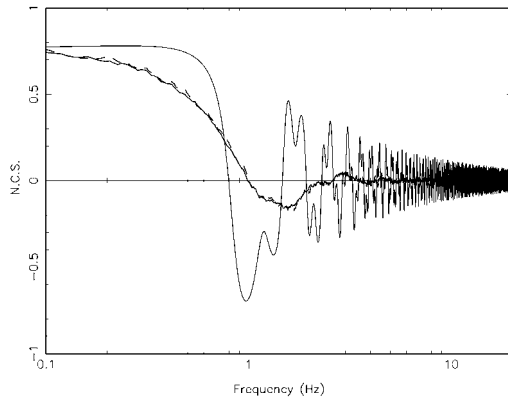


**Fig. 7** NCS spectra with  $V=300$  km s<sup>-1</sup>. Thin solid line:  $\sigma/V=0.0$ ; thick solid line:  $\sigma/V=0.6$  with symmetrical cuts; thick dash line:  $\sigma/V=0.6$  with asymmetrical cut.

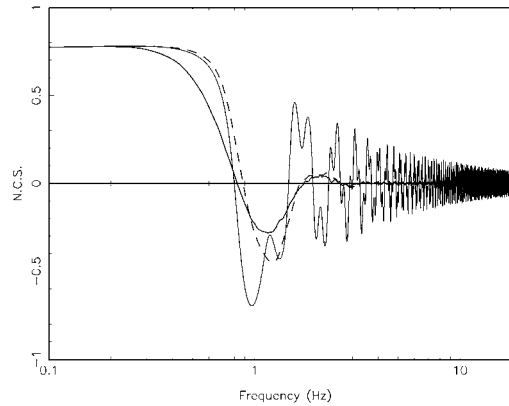


**Fig. 8** NCS spectra with  $V=300$  km s<sup>-1</sup>. Thin solid line:  $\sigma/V=0.0$ ; thick solid line:  $\sigma/V=0.3$  with symmetrical cuts; thick dash line:  $\sigma/V=0.3$  with asymmetrical cut.

The observed results indicate that  $\sigma/V$  probably does not exceed 0.5 if the point  $P$  (in Fig. 1) is not too near the Sun (Tokumaru et al. 1994; Ekers & Little 1971). Figures 7 and 8 present the results of simulations with different  $\sigma/V$  values. Figure 7 ( $\sigma/V = 0.6$  random distribution with asymmetry and asymmetry cuts) shows that the factor  $K$  is about 0.8, which is consistent with Table 2. In Figure 8 the input speed distribution has  $\sigma/V = 0.3$ . The results from these simulations are: (1) error < 10% with asymmetry cut and (2) error < 5% with symmetry cut.

In summary, the SSDF is a useful observing technique for studying the IPS with advantage and a new system at the NAOC will be the IPS monitoring instrument of the National Meridian Project.

### 2.3 Data Reduction of NCS Technique

Let the two data sets obtained from a dual-frequency simultaneous IPS observation be DAT1 and DAT2 (source on). To obtain a Nyquist frequency of 20 Hz, DAT1 and DAT2 will be convolved respectively to DAT1N and DAT2N with a rectangular window of suitable width corresponding to a re-sampling rate of 40 Hz if the original sampling rate is faster than 40 Hz. For example, the width should be five times the

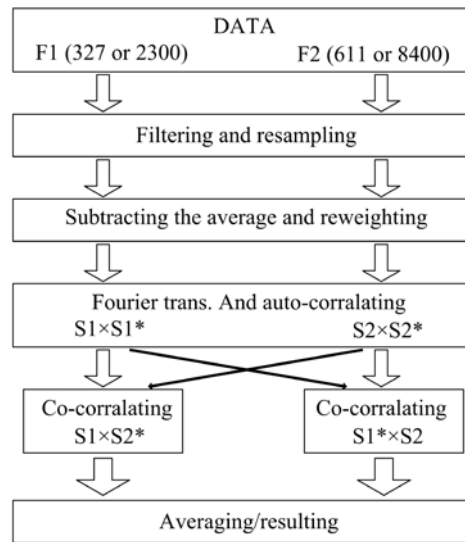


**Fig. 9** A flow chart of the NCS technique data reduction.

original sampling interval if the original sampling rate is 200 Hz. The raw data sets DAT1N and DAT2N will then be broken into subsets of length 512 sample points and the bad data polluted by interference and DC jump will be rejected. Then, the receiver gain will be adjusted if necessary. The means of each subset will be subtracted and the subset is multiplied by a triangular weighting function, which is unity at the center falling to zero at both ends. This is to reduce the cut-effects of the Fourier transform (FT). Finally, FT will be performed on the subsets at two frequencies and two polarizations.

In total, four auto-correlation spectra will be obtained by multiplying the real part of each transformed series by its conjugate ( $S_n \times S_n^*$ ) and four cross-correlation spectra, by multiplying the real part of each transformed series by the conjugate of the other transformed series ( $S_m \times S_n^*$ ). These spectra acquired from each subset are then averaged to produce the final spectra. Figure 9 shows the data reduction procedure.

A simplified procedure is applied to the data of source off observations. Scintillation indices can be calculated from the means of all adopted data of source-on and source-off observations.

## 2.4 Comparing the SSDF Technique with the SSSF Method

The SSSF method of IPS observation has been studied by quite a number of authors (e.g., Manoharan et al. 1990; Ma 1993). Figure 10 shows an example of IPS spectrum obtained by the Miyun telescope, NAOC (Zhang et al. 2001; Wu et al. 2001). To acquire the solar wind velocity from this spectrum, two approaches can be taken: One is spectral multi-parameter model-fitting, and the other is calculation of the characteristic frequencies (Ye & Qiu 1996).

The model fitting method used in an SSSF IPS spectrum is a multi-free-parameter fitting which suffers from the selection effect. In addition, the SSSF model fitting needs a higher signal to noise ratio (better than 25 dB) to obtain reasonable fitting results (Tokumaru et al. 1994).

The method of calculation of the characteristic frequency is first to find out the frequency  $f_F$  corresponding to the Fresnel point ("Fresnel knee"), and then to calculate the solar wind speed by the formula  $V = f_F \sqrt{\pi \lambda Z}$ . Now the spectrum around the Fresnel knee is very smooth (refer to Fig. 10), so  $f_F$  has a larger uncertainty. The second method for isotropic solar wind is only to find the frequency  $f_{\min}$  corresponding to the first minimum of the spectrum and then using the formula  $V = f_{\min} \sqrt{\lambda Z}$  to calculate the solar wind speed (Ma 1993). Both observation and theoretical study have shown that the Fresnel knee becomes more ambiguous when the axial ratio of solar wind increases and because the noise the first minimum is also less clear, especially for observation at large elongation angle  $\epsilon$  or a large AR, for example, the Fresnel oscillation will not appear when the elongation angle  $\epsilon \geq 40^\circ$ , i.e., there would be no minimum point.

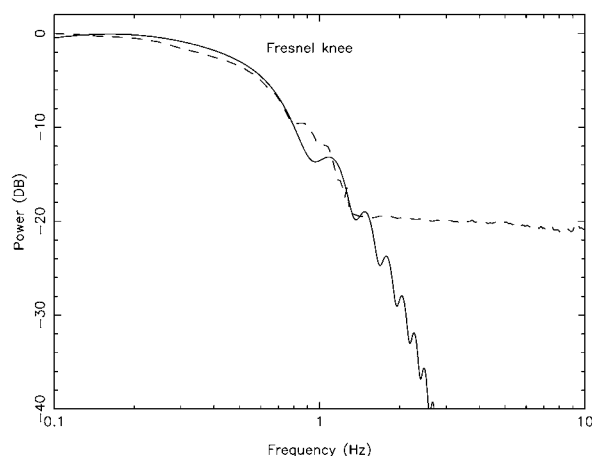


**Fig. 10** Observed IPS spectrum (dash line) and the fitted spectrum (solid line) obtained by the Miyun telescope, NAOC, by using the SSSF method. The fitted parameters are  $v = 400 \text{ km s}^{-1}$ ,  $\text{AR} = 2.3$ ,  $\theta = 0.2''$  and  $\alpha = 3.5$ .

### 3 THE NEW SSDF SYSTEM AT THE NAOC

A new receiving system for SSDF IPS observation at the NAOC is now under construction, which is a dual-frequency front-end and a dual-channel multi-function back-end to be equipped to the 50 m parabolic radio telescope. The flow chart of this system is shown in Figure 11. The integration time of the receiver system should be sufficiently short since the IPS phenomena varies rapidly. This implies that the effective receiving area of the IPS antenna should be large enough to ensure the system has a good instant sensitivity and its band-width should match well the system time resolution. Good low noise amplifiers (LNA) are needed to reduce the system noise level and so it is better to install them as close as possible to the feeds. Because most IPS sources are randomly polarized, so polarization observation of IPS is not very important, and observation with full polarization makes it possible to increase the system's sensitivity. Figure 12 shows the 50 m antenna, and Figure 13 shows the dual-frequency feeds including the small calibration feeds. The main system parameters are listed in Table 3.

There are two dual-frequency groups available in the system. One is 327/611 MHz and the other is 2300/8400 MHz. A frequency synthesizer is used as the LO so that the receiving frequency can be adjusted slightly around the central frequencies (327/611 MHz) to dodge any strong interference. This operation can be done because the feeds have wide bands and the working bands are narrow, e.g., the band width of the 327 MHz feed is 35 MHz, and the working band width at 327 MHz is about 4 MHz. We found that there are some relative quiet areas, with less of strong interference, around 611 MHz (Fig. 14). We have monitored the radio environment at the telescope site by using the 50 m telescope with a spectrometer for all directions

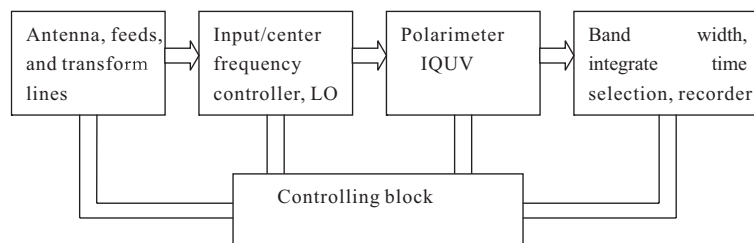


**Fig. 11** Block chart of the new SSDF at the NAOC.



Fig. 12 Fifty-meter parabolic radio telescope at the Miyun Station, NAOC.



Fig. 13 Left: 327/611 MHz feed; Right: 2300/8400 MHz feed.

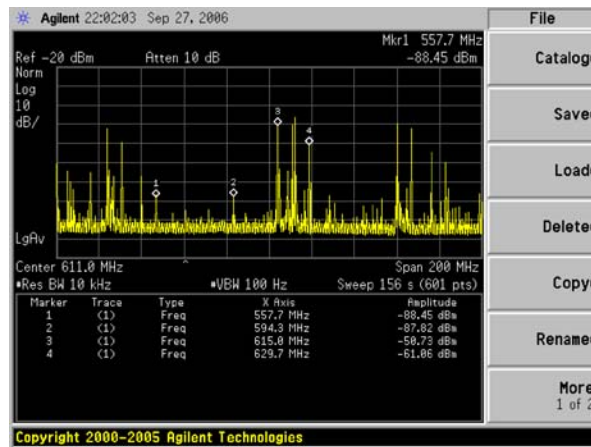


Fig. 14 Spectrum around 611 MHz recorded by the 50 m telescope (Piao & Zhang 2006, private communication).

**Table 3** Main Parameters of the Antenna and SSDF System

Aperture / F/D	50 m / 0.35
Antenna efficiency (327/611/2300 MHz 50 m, 8400 MHz 43 m)	>0.5
Gains at 327/611/2300/8400 MHz	43/48/60/68 dB
Frequency group	327/611, 2300/8400
Band width	2/4/8/20 MHz
Sampling interval	20 ms
System noise level	327/611, 70 K; 2300/8400, 60 K
Minimum measurable temperature(1.2 s/8 MHz)	25 mK/10 mK

around the telescope. No serious interference was found in the S/X bands, and it is easy to find areas 80 MHz wide around 2300/8400 MHz. Regular monitoring programs are being planned for the future.

Two selectable observing modes with this SSDF system are (1) Tracking a scintillation source for a long time to obtain information of IPS at an almost constant distance to the Sun, i.e. to monitor the time variation of the solar wind; (2) Observing the scintillation sources one by one around the Sun to obtain information on the space distribution of the solar wind. The new SSDF system can observe radio sources stronger than 1 Jy ( $SN > 5$ ), through which many sources have been found.

#### 4 SUMMARY

Results of this study suggest that, compared to the SSSF method, the SSDF technique has the following advantages: (1) Higher accuracy in the calculation of the characteristic frequency; (2) Small effects from the variation of the solar wind parameters; (3) Higher sensitivity. The only additional cost for the SSDF technique is for the receiver development.

The new receiving system for SSDF IPS observation at the NAOC is now under construction with the installation of a dual-frequency front-end and dual-channel multi-function back-end onto the 50 m parabolic radio telescope. There are two dual-frequency groups available in this system: 327/611 MHz and 2300/8400 MHz. This IPS observation facility is a group member of the National Meridian Project.

**Acknowledgements** The author thanks Senior engineer Piao Tingyi and Prof. Zhang Hongbo, for their help on the interference monitoring and providing Figure 14 of the present paper.

#### References

- Asai K., Ishida Y., Kojima M. et al., 1995, *J. Geomag. Geoelectr.*, 47, 1107  
 Ekers R. D., Little L. T., 1971, *AAP*, 10, 310  
 Hewish A., Scott P. F., Wills D., 1964, *Nature*, 203, 1214  
 Manoharan P. K., Ananthkrishnan S., 1990, *MNRAS*, 244, 691  
 Ma G. Y., PhD Thesis, 1993, 45  
 Purvis A., Tappin S. J., Rees W. G. et al., 1987, *MNRAS*, 229, 589  
 Scott S. L., Rickett B. J., Armstrong J. W., 1983, *A&A*, 123, 191  
 Swarup G., Sarma N. V. G., Joshi M. N. et al., 1971, *Nature Physical Science*, 230, 195  
 Tokumaru M., Kondo T., Mori H. et al., 1994, *J. Geomag. Geoelectr.*, 46, 835  
 Vitkevich V. V., Glushaev A. A., Iliasov Iu. P. et al., 1976, *Radiofizika*, 19, 1594  
 Wu J. H., Zhang X. Z., Zheng Y. J., 2001, *Ap&SS*, 278, 189  
 Ye P. Z., Qiu Y. H., 1996 *Acta Astrophysica Sinica*, 16, 389  
 Zhang X. Z., Wu J. H., Chen H. S. et al., 2001, *Kexue Tongbao*, 46, 1081